Scalable time-correlated photon counting system with multiple independent input channels

Michael Wahl,[1,a)] Hans-Jürgen Rahn,[1] Tino Röhlicke,[1] Gerald Kell,[2] Daniel Nettels,[3] Frank Hillger,[3] Ben Schuler,[3] and Rainer Erdmann[1]
[1]*PicoQuant GmbH, Rudower Chaussee 29, D-12489 Berlin, Germany*
[2]*Fachhochschule Brandenburg, Magdeburger Str. 50, D-14770 Brandenburg, Germany*
[3]*Biochemisches Institut, Universität Zürich, Winterthurerstrasse 190, CH-8057 Zürich, Switzerland*

(Received 11 July 2008; accepted 3 December 2008; published online 29 December 2008)

Time-correlated single photon counting continues to gain importance in a wide range of applications. Most prominently, it is used for time-resolved fluorescence measurements with sensitivity down to the single molecule level. While the primary goal of the method used to be the determination of fluorescence lifetimes upon optical excitation by short light pulses, recent modifications and refinements of instrumentation and methodology allow for the recovery of much more information from the detected photons, and enable entirely new applications. This is achieved most successfully by continuously recording individually detected photons with their arrival time and detection channel information (time tagging), thus avoiding premature data reduction and concomitant loss of information. An important property of the instrumentation used is the number of detection channels and the way they interrelate. Here we present a new instrument architecture that allows scalability in terms of the number of input channels while all channels are synchronized to picoseconds of relative timing and yet operate independent of each other. This is achieved by means of a modular design with independent crystal-locked time digitizers and a central processing unit for sorting and processing of the timing data. The modules communicate through high speed serial links supporting the full throughput rate of the time digitizers. Event processing is implemented in programmable logic, permitting classical histogramming, as well as time tagging of individual photons and their temporally ordered streaming to the host computer. Based on the time-ordered event data, any algorithms and methods for the analysis of fluorescence dynamics can be implemented not only in postprocessing but also in real time. Results from recently emerging single molecule applications are presented to demonstrate the capabilities of the instrument. [DOI: 10.1063/1.3055912]

I. INTRODUCTION

The time-correlated single photon counting (TCSPC) method is based on the repetitive, precisely timed registration of single photons, e.g., of a fluorescence signal. Historically, the primary goal of TCSPC was limited to the determination of fluorescence lifetimes, usually upon periodic excitation by a short flash or laser pulse. A photon detector provides electrical timing signals; the reference for this photon timing is the corresponding excitation pulse (also referred to as synchronization or sync signal). The TCSPC electronics has to record each emitted photon with great precision relative to the corresponding synchronization event. A histogram of the resulting intervals reflects the fluorescence decay of the observed molecule or ensemble.[1]

The time difference measurement in TCSPC is obtained by means of fast digital timing electronics. High demands on time resolution exist in fluorescence lifetime measurements on organic dyes used for the fluorescent labeling of biological macromolecules. Here, the required time resolution can be on the order of a few picoseconds. Historically, the most common picosecond timing solution was the combination of time to amplitude converters (TACs) and analog to digital converters (ADCs), allowing time bin widths of less than a picosecond. Recently, dedicated time measurement circuits, so-called time to digital converters (TDCs) are approaching similar time resolution, with substantially extended measurement range, crystal locked calibration, and benefits in system integration.[2]

In TCSPC histogramming the only information in the temporal pattern of photon arrival times that is used is the time between pulsed dye excitation and subsequent photon emission, i.e., information mostly found on a picosecond to nanosecond scale. It was soon realized that an extension of these time scales is of great value in the context of single molecule fluorescence detection and spectroscopy. For instance, a method that makes use of fluctuations in photon arrival times over a wide time range is fluorescence correlation spectroscopy (FCS). From the fluorescence intensity fluctuations of molecules diffusing through a confocal volume, one can obtain information, e.g., about the translational diffusion constant and the number of molecules in the observed volume.[3] To obtain the time resolution of interest for the diffusion processes, photon counting with microsecond

[a)]Author to whom correspondence should be addressed. Electronic mail: wahl@picoquant.com.

time resolution is required. Hardware correlators for FCS can be implemented very efficiently and are widely used.[4] However, they are dedicated to correlation with nanosecond resolution at best and cannot perform picosecond TCSPC.

Photon coincidence correlation techniques can be used to observe photon antibunching effects on the picosecond to nanosecond time scale[5,6] and have recently been used to determine the number of emitters per molecule or molecular complex.[7–10] These techniques require a time resolution similar to classical TCSPC and cannot be performed with typical FCS instrumentation. Similar approaches can be used to obtain dynamics information on the nanosecond time scale.[11–13]

In summary, the requirements of virtually all of these analytical techniques based on single photon arrival times are very similar, but they extract information on very different time scales, thus calling for unified instrumentation. A first step toward this end was a modification of classical TCSPC electronics. The start-stop timing circuitry is used as previously, providing the required picosecond time resolution for TCSPC. In order to maintain the information embedded in the temporal patterns of photon arrivals, the events are stored as separate records. In addition, a coarser timing is performed on each photon event with respect to the start of the experiment. First implementations of this concept referred to it from an application perspective, coining the term burst integrated fluorescence lifetime.[14] More generally, it is referred to as time-tagged time-resolved (TTTR) data collection.[15]

The time-tagging concept avoids both redundancy in the data stream and loss of information. As a result, virtually all algorithms and methods for the analysis of fluorescence dynamics can be implemented. For instance, intensity traces over time, as traditionally obtained from multichannel scalers, are obtained from time-tagged data by evaluating only the time tags of the photon records. This provides access to fluorescence bursts from freely diffusing single molecules or to blinking dynamics.[16,17] The time-tagged data format also allows the combination of high and low resolution timing with the detector channel information.[18] This combined information proves very powerful in the investigation of molecular dynamics, e.g., in protein interaction.[19]

An advantage of off-line analysis of time-tagged photon event data is that the type of analysis does not have to be defined at the time of measurement. A good example is FCS: Traditional hardware correlators perform an immediate (real-time) data reduction that does not conserve the original data, and thus excludes alternative types of data analysis. Having individual photon records available, one can perform the correlation using suitable software and select from a wide range of analysis methods without the need for additional measurements. On modern computers and with recently developed fast algorithms, it is also possible to perform the correlation in real time.[20] By using the information of TTTR-type data, subpopulation-selective[21] or time-gated[22] intensity correlations can be calculated, and different molecular species in a mixture can be separated from a single FCS measurement. By filtering the photon events according to their TCSPC time before the correlation procedure, one can obtain separate FCS curves for each species.[23] Another application of time-tagged TCSPC is fluorescence lifetime imaging (FLIM), for which the spatial origin of the photons must be recorded in addition to the TCSPC data. FLIM systems using on-board histogramming suffer limits in the recordable image size. To avoid this, we previously extended the TTTR data stream concept to contain markers for synchronization information from a scanner,[24] allowing the reconstruction of two-dimensional or three-dimensional images from the stream of TTTR records. The data are nearly free of redundancy and can therefore be transferred in real time, even if the scan speed is very fast, e.g., in laser scanning microscopes.[25]

In the original TTTR approach, the different time scales are processed and used independently. However, often it is of great interest to obtain high resolution timing on the overall scale, i.e., combining coarse and fine timing into one global arrival time per event, with picosecond resolution. It has been demonstrated that it is possible to combine coarse and fine timing in order to perform temporal analysis from the picosecond to second time scale.[26] In a more general approach, without assumptions on start and stop events, one collects precise time stamps of all events of interest (excitation, emission or others). It is then possible to perform the desired analysis on the original event times, thereby covering almost all dynamic effects of the photophysics and other dynamics of fluorescent molecules. Ideally, this is done on independent channels, such that detector dead time effects can be eliminated by cross correlating the signals.[27]

II. INSTRUMENT

A. New requirements

A limitation of the existing TCSPC instrument designs is the number of independent input channels. In order to work with signals from multiple detectors (e.g., color channels) or recently emerging detector arrays,[28–30] large numbers of inputs ranging from a few to some tens of inputs are of immediate practical interest. On the other hand, the individual needs of research groups vary and usually grow with time, while initial budgets are often limited. This calls for a scalable design that until now did not exist. Existing commercial solutions that multiplex several detector signals into one timing input rely on a low probability of receiving photons on more than one channel at the same time.[31] Any such multihits they must discard due to ambiguity. The multiplexed channels are therefore not independent, which causes artifacts in correlation measurements. While the most prominent artifact is a gap in the correlation curves at lag times shorter than the dead time, more subtle and easily overlooked artifacts result from "blinding" other channels when one channel receives high photon rates. For similar reasons, a multiplexing architecture forbids applications with high count rates, such as optical tomography or fast FLIM with multiple color channels. Furthermore, the multiplexing concept is limited to a few channels.

Another important application calling for independent channels is the determination of the number of emitters by means of photon antibunching measurements. Counting the number of fluorescent probes within a confocal observation volume has even been demonstrated in living cells.[32,33] How-

ever, the method is limited to a maximum of about three to four molecules when using a standard detection scheme with two detectors. Recent work indicates that an extension of the method by use of more detection channels should allow to count higher numbers of molecules.[34] Extension of the counting range beyond ten would be extremely valuable in cell biology as it would allow a quantitative investigation of protein complexes and other molecular aggregates in cells.

Existing solutions providing multiple truly independent channels do so by operating multiple TCSPC units in parallel, where each unit has one photon input channel and one synchronization input channel.[35] This requires fanning out the synchronization signal to each unit. In time-tagging data collection, this causes severe problems in assigning simultaneous events from two or more channels to the correct sync period because inevitably there are tolerances in the sync timing. An ideal solution should allow scaling of the number of independent photon timing channels, all operating against one common synchronization input channel. Furthermore, parallel operation of complete TCSPC units, each with their own host computer interface, will result in multiple data streams arriving at the host computer. Relative timing between events across channels is not immediately possible. This will cause complications in real-time analysis of time-tagged data where the order and temporal relation of events across all channels is critical. Ideally, the instrument should deliver one single data stream with all events from all channels in correct temporal order.

B. Design features

The chosen new architecture is modular in order to obtain a scalable system in terms of the number of input channels, while using one common synchronization channel, and furthermore, to obtain a single output data stream that contains time-tag records for all events from all inputs in correct temporal order, despite any variations in event rates across the channels. Another key objective is unlimited and uninterrupted real-time recording of this data stream at full resolution of the timing circuits, even at high event rates.

The complete instrument contains multiple TDC based input timing units that may each have one or more timing signal inputs. Scalability is achieved by implementing the device as a frame with multiple slot modules so that the number of input timing units can be chosen according to application needs. The internal data formats, data links, and processing logic are laid out for immediate scalability to a maximum of 64 channels. The first physical implementation of the housing is laid out to accommodate a maximum of two detector input timing units, each providing two channels and a separate input timing unit for the synchronization channel. Next generation modules and housings can extend the number of detector channels without any change in data formats and processing logic.

The TDC circuitry uses a hybrid design combining field programmable logic with custom integrated circuits in SiGe technology.[36] The timing resolution of the TDCs is 1 ps. One input timing unit is dedicated to a synchronization channel. This specialized module has a timing input identical to those of the detector channels, and additional inputs for other signals that are captured at lower resolution and get inserted in the data stream exactly like photon events. These low resolution signals serve as markers for different types of synchronization, e.g., representing spatial information of scanning devices. A central crystal clock and a clock distribution system ensure that the timing units have a common time base. This does not necessarily require the same clock frequency to be used in all units. Phase-locked loops are used to provide synchronous clocks in all units. Similarly, the central clock may be fed in from an external source such as an atomic clock. Multiple high speed serial links are used for data communication between each timing unit and a main processing unit. The input timing units contain first in first out (FiFo) buffers for the event records to be sent to the high speed serial links. Using serial links is an important prerequisite for the desired scalability of the system at reasonable cost. The main processing unit also contains FiFo buffers for the event records coming from the serial links. The FiFo buffers are an important prerequisite for the desired continuous and uninterrupted operation at high event rates. However, they introduce a temporal decoupling of the event records. Since the event rates on the individual input channels can be extremely different (or even zero), the time-tagged event records delivered to the main processing unit arrive unpredictably disordered. The actual arrival time of the records is no longer in accordance with the original event times. However, such an order is required in the data stream to the host computer because the latter is usually processing these data on the fly in real time. The processing algorithms are typically very demanding so that ordered data are a strict requirement. The present design comprises a specialized sorter that solves this problem. Sorting generally requires the comparison of values. This is trivial when all values are available, e.g., in the main memory of a computer. In the special case here, these are timing figures that are continuously streamed through the sorter. Since there is a limited amount of buffer memory, the timing values to be compared may not be present in the buffer, unless suitable measures are taken. This is solved as follows. Since the data format of the event records delivered from the timing units is limited, special overflow records are introduced when such overflows occur. This concept was originally conceived to recover the original event data on the host computer.[15] However, the present instrument uses the overflow records to solve the problem of sorting by interpreting them as boundaries of "frames" in which the availability of timing data is always valid for comparison. This does not require recovering the original event data. The FiFo buffer before the sorter is chosen such that the maximum amount of data that can possibly arrive between two successive overflows can be held. This amount of data is small enough to perform real-time sorting at the highest event rates that experiments typically deliver, currently some tens of megahertz. The main processing unit also comprises a FiFo buffer for the sorted event records to be sent to the host computer interface. This ensures that sorting and other processing is decoupled from the temporal structure of the host transfer process. Furthermore, the main processing unit comprises an overall measurement and data flow controller that takes commands from the host computer

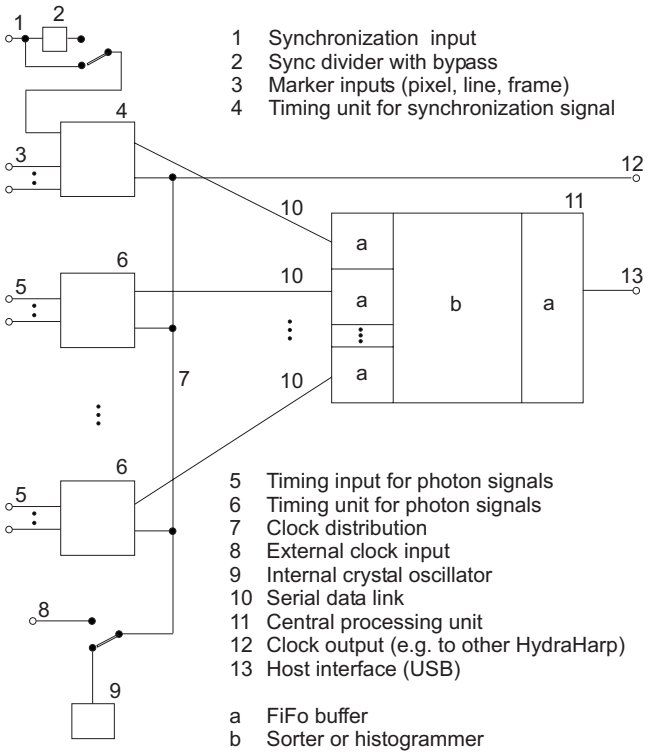

FIG. 1. Block diagram of the instrument architecture. Dots between identical building blocks denote scalability.

and signals any conditions the host may need to be informed of. The processing performed in the timing units and in the main processing units is implemented in programmable logic. While the input timing units are operated in a fixed configuration, the main processing unit is reconfigurable at runtime to allow different measurement modes (see Sec. II C).

Figure 1 shows a block diagram of the instrument architecture. All timing inputs have a constant fraction discriminator in order to handle fluctuating pulse heights. A divider in the synchronization channel can be used if high sync frequencies are present; otherwise it is bypassed. All timing units are locked to the same crystal clock so that their time measurements are always synchronized and equally calibrated. The event timings may be regarded as precise (picosecond) wall clock readings. Therefore, the subtraction or comparison of event times is valid within and across all channels. Because of the TDC based time measurement, the time difference between events (e.g., start and stop) can be arbitrarily long, while still being determined at the full resolution. Relative error is determined only by the crystal and clock distribution characteristics. Another feature resulting from the independent channels is that arbitrary offsets can be introduced in each channel at picosecond resolution, thereby completely eliminating the need for cable delay adjustments as known from traditional TAC based systems.

C. Data acquisition schemes

A conventional histogramming mode supports classical TCSPC applications such as fluorescence lifetime measurements. This is implemented in hardware so that the full input rate of each channel (1/dead time) can be processed. In theory the start-stop time spans are unlimited. Only due to practical limits of the histogram storage, the histogramming mode is limited to 65 535 time bins. The bin width can also be increased (binary multiples of the 1 ps base resolution) in order to increase the overall time span (here up to 65 μs). Since the dead time is acting only within each channel, at slow excitation rates the histogrammer can process multiple photons per excitation/emission cycle. Hence, it can collect data much more efficiently than a TAC based system, which always needs to wait for the next stop event.

Apart from the classical histogramming mode, the system provides two time-tagging data acquisition modes introduced previously.[27] The difference in the two time-tagging modes (T2 and T3 modes) is primarily in the handling of sync events from, e.g., a pulsed laser. In T2 mode, all detector signal inputs are functionally identical. Usually all inputs are used to connect photon detectors. The divider is bypassed. The events from all channels are recorded independently and treated equally. In each case an event record is generated that contains information about the channel it came from, and the arrival time of the event with respect to the overall measurement start. The timing is recorded with 1 ps resolution. Each T2 mode event record consists of 32 bits carrying the channel number and a time tag. If the time tag overflows, a special overflow marker record is inserted in the data stream so that upon processing of the data stream a theoretically infinite time span can be recovered at full resolution. Autocorrelations within a channel can therefore be calculated at the full resolution, but only starting from lag times larger than the dead time ($<$80 ns). However, dead times, including those of the detectors, exist only within each channel but not across the channels. Therefore, cross correlations can be calculated down to zero lag time. This allows powerful applications such as FCS with lag times from picoseconds to hours.

The T2 event records are queued in a FiFo buffer capable of holding up to 2 097 152 event records. The FiFo input is fast enough to accept records at the full speed of the time digitizers (up to 12.5 Mcounts/s each). This means that even during an intense burst of photons, no events will be dropped except those lost in the dead time. The FiFo output is continuously read by the host PC, thereby making room for new incoming events. Even if the average read rate of the host PC is limited, bursts with much higher rate can be recorded for some time. Only if the average count rate over a longer period of time exceeds the readout speed of the PC, a FiFo overrun could occur. Then the measurement must be aborted because data integrity cannot be maintained. However, on a modern PC (AMD Athlon 64$\times$2 4600+, WINDOWS XP), sustained average count rates over 9 Mcounts/s were obtained. This total transfer rate must be shared by all input channels. For all practically relevant fluorescence detection applications, the effective rate per channel is more than sufficient because single photon statistics are the limiting factor.

In T3 mode, the sync channel is connected to a periodic synchronization signal, typically from an excitation source. As far as the experimental setup is concerned, this is the same as in TCSPC histogramming mode. The main objective is to allow high sync rates from mode-locked lasers (up to

150 MHz) which could not be handled in T2 mode due to dead time. Accommodating the high sync rates in T3 mode is achieved by means of a sync divider as introduced previously.[27] The event records in T3 mode are composed of two timing figures: (1) the start-stop timing difference between the photon event and the last sync event, and (2) the arrival time of the event pair on the overall experiment time scale (the time tag). The time tag is obtained by counting sync pulses. From the T3 mode event records, it is therefore possible to precisely determine which sync period a photon event belongs to. Since the sync period is also known precisely, this furthermore allows reconstructing the arrival time of the photon with respect to the overall experiment time.

Each T3 mode event record consists of 32 bits carrying the channel number, the start-stop time, and the sync count. If the sync count overflows, a special overflow marker record is inserted in the data stream so that upon processing of the data stream a theoretically infinite time span can be recovered. 15 bits of the record are used for the start-stop time difference, covering a time span of $32768 \times R$, where R is the chosen resolution. At the highest possible resolution of 1 ps this results in a span of 32 ns. If the time difference between photon and the last sync event is larger, the photon event cannot be recorded. This is the same as in histogramming mode, where the number of bins is also finite. However, by choosing a suitable sync rate and a compatible resolution R, it is possible to reasonably accommodate all relevant experiment scenarios. R can be chosen in doubling steps between 1 and 1024 ps. The data transfer uses the same FiFo buffer as in T2 mode. Again, sustained average count rates over 9 Mcounts/s are obtained. In T3 mode this total transfer rate is fully available for the detector input channels since the sync events are handled implicitly.

The throughput limit of 9 Mcounts/s in the time-tagging modes results from the bandwidth limit of the USB 2.0 interface. It corresponds to a throughput of 36 Mbytes/s that is fully exploiting the practical limits of USB 2.0 in the presence of overhead at the protocol and operating system level. At the current level of physically implemented scaling to four channels, this bandwidth is more than sufficient since photon rates are limited by single photon statistics. Assuming full scaling of the system to the architecture limit of 64 channels would reduce the throughput per channel to 140 kcounts/s. While this is still sufficient for single molecule studies including the important coincidence correlation experiments, it would limit high throughput applications such as optical tomography. However, especially optical tomography is commonly performed in histogramming mode, where the USB bandwidth is only of relevance during the retrieval of the histograms from the on-board memory, where time is not critical. For applications with high throughput demands in time-tagging mode, it is anticipated to migrate the host interface to a bus system with higher bandwidth such as peripheral component interconnect express (PCIe) over cable or USB 3.0.

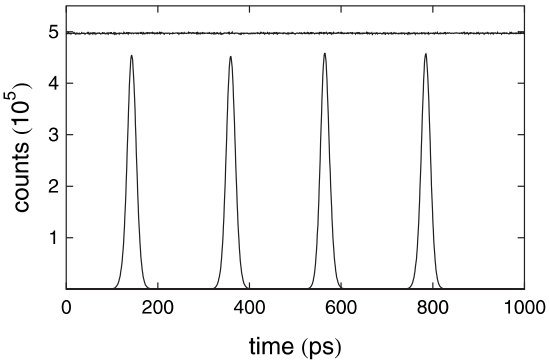

FIG. 2. Results of intrinsic performance measurements: DNL (flat line) and timing jitter in four channels (peaked histograms).

III. EXPERIMENTAL RESULTS

A. Instrument performance and timing accuracy

The current implementation of the described TCSPC system (HydraHarp 400, PicoQuant) was used in various measurement scenarios to verify functionality and timing accuracy. Although the digital resolution of the instrument is fixed at 1 ps by the TDC design, a timing uncertainty (jitter) due to noise is always present. This is true even for digital signals because of the finite slope of any signal transition. In order to test this quantity for the present instrument, the following test was performed. A test generator (CG635, Stanford Research Systems) provided pulses of 1 MHz repetition rate. This signal was fanned out through a reflection free splitter so that five identical signals were obtained. These were fed to the sync input and four input channels of the device under test, using approximately identical cable lengths. The device was then operated in histogramming mode, where the time differences between sync input and the respective channel are recorded. The result is shown in Fig. 2. Each peak represents the histogram obtained for one channel. Using the software adjustable offset of each channel, the spacings between the peaks were set arbitrarily. Numerical analysis of the distributions shows that the time jitter is typically 10 ps rms. It should be noted that this is the overall error including the sync channel and the respective detector channel.

An intrinsic system property with relevance, e.g., for fluorescence lifetime measurements is differential nonlinearity (DNL). In order to test this, another standard experiment was performed. A test generator (CG635, Stanford Research Systems) providing pulses at 120 MHz was used as the sync signal. The high rate allows for shorter measurement times. A second generator (DS1090, Dallas Semiconductor) provided a 1 MHz pulse train with 8% dithering in frequency which was amplified and fed to one of the detector input channels. The use of independent generators, and additionally one of them dithering its period, ensured that from the perspective of the device under test, the signals were effectively uncorrelated. Therefore, the expected histogram of time differences should be evenly filled. Any deviation from a flat line would be due to either residual error of counting statistics or systematic error reflecting DNL. In order to make the residual error of counting statistics as small as possible (within reasonable limits of measurement time) the ex-

TABLE I. Long span timing accuracy and jitter for different time spans within and across channels (all in nanoseconds).

	Measured within channel (ns)		Measured across channels (ns)	
Gen. period (ns)	Mean	Standard deviation	Mean	Standard deviation
10^3	999.996 575	0.008 59	994.855 306	0.010 34
10^4	9999.965 97	0.009 73	9994.821 91	0.010 15
10^5	99 999.6601	0.010 37	99 994.5202	0.010 37
10^6	999 996.655	0.011 18	999 991.512	0.010 83

periment was allowed to run until the largest count had reached 500 000. The result is shown as the flat line in Fig. 2. Numerical analysis results in a rms deviation of 0.15% from the average. Calculating the expected error due to counting statistics for the count level of 500 000 one obtains an expected relative error of 0.14%. It may therefore be assumed that the error due to DNL is still much smaller than the statistical error. This result is very good compared to instruments based on TAC/ADC combinations and may be attributed to the TDC based design in combination with the independent operation of the timing channels.

Another intrinsic instrument parameter is integral linearity. Because of the clock-based design, integral linearity is essentially governed by the clock crystal characteristics. Nevertheless, a basic test was performed to show that the picosecond timing performance can be maintained even at long time spans both in terms of linearity and jitter. The test generator CG635 used previously is specified for a period jitter of <1 ps in the range of 1 KHz–5 MHz. It was set to emit a pulse train, which was split into two identical signals. These were fed to two input channels of the device under test. Timing data were then collected in T2 mode. Analyzing the data by software allowed calculating time differences within the channels and across the channels. By measuring repeatedly over a whole generator period, the long span characteristics can be obtained. Table I shows the results including the standard deviations. The average periods are obtained with an accuracy of five decimal places as expected for the accuracy of the crystal of the device under test. This can be improved by using an external clock, e.g., from an oven controlled crystal oscillator or an atomic clock. Note that the constant offset of ~ 5 ns in the measurements across channels is due a deliberate delay. It was introduced only to simplify data analysis. The standard deviations are in agreement with the results for the short span timing uncertainty. As expected, there is a small trend toward larger errors at larger time spans. Nevertheless, the error is eight orders of magnitude smaller than the longest time span measured.

Apart from the fundamental tests with generator signals, fluorescence lifetime measurements were performed with dyes of known lifetime. Results in accordance with published values were routinely obtained.

B. Single molecule studies

Here we present two applications of the new instrument that benefit greatly from the availability of independent, but synchronized input channels. The data presented in this section were measured using a MicroTime 200 confocal microscope (PicoQuant) equipped with a cw solid-state diode-pumped laser (Coherent, Sapphire 488-200) operating at 488 nm, a 1.2 numerical aperture, 60× microscope objective (Olympus UplanApo 60×/1.20 W), and a 100 μm confocal pinhole. The fluorescence photons collected by the objective were distributed onto up to four detectors (PerkinElmer Optoelectronics SPCM-AQR-15) by means of appropriate beam splitters (e.g., 50/50 beam splitters, polarizing beam splitters, or dichroic mirrors). Each detector was connected to one of the four independent TCSPC channels of the HydraHarp 400 operated in its T2 mode. The fluorophore-labeled, dissolved sample molecules were freely diffusing through the confocal volume of the instrument.

First, we show that data acquired with the HydraHarp 400 can be used to obtain correlation functions from picoseconds to seconds and, in particular, that they can be used to measure the rapid rotational diffusion of biomolecular complexes. As an example, we use the stable complex of the protein rhodanese with the molecular chaperone GroEL.[37] Molecular chaperones are a class of proteins that assist other proteins during folding.[38] Topics of particular interest are the non-native structure and the conformational dynamics of rhodanese upon binding to GroEL, and the properties of the extremely stable rhodanese-GroEL complex. For the data shown here, the chaperone-bound rhodanese was labeled with a single Alexa 488 dye (Invitrogen) and observed freely diffusing in solution at a concentration of 1 nM. Fluorescence was monitored polarization selectively by separating the components of parallel and perpendicular polarization with respect to the linear polarization of the excitation light. Subsequently, the photons of each component were randomly distributed to a pair of detectors by means of a 50/50 beam splitter. This Hanbury-Brown and Twiss[39] configuration allows the calculation of autocorrelation data for lag times smaller than the dead times of the detectors. Figure 3 shows correlations obtained from a single measurement (10 h integration time), where $G_{\parallel\parallel}(\tau)$ is the autocorrelation of the parallel polarized photons, and $G_{\parallel\perp}(\tau)$ is the cross correlation between parallel and orthogonal polarized photons. Figure 3(a) represents the correlation data over a time range from one hundred picoseconds to one second on a logarithmic time scale. Figure 3(b) shows the same results restricted to the nanosecond range and on a linear time scale with 1 ns binning. [Note that for obtaining negative lag times as in Fig. 3(b), no hardware delay lines are needed, in contrast to conventional FCS and Hanbury-Brown and Twiss instruments.]

$G_{\parallel\parallel}(\tau)$ and $G_{\parallel\perp}(\tau)$ are virtually identical for lag times longer than 1 μs. Both exhibit decay components in the millisecond and 10 μs range, which can be attributed to translational diffusion of the rhodanese-GroEL complex through the confocal volume and to triplet blinking of the Alexa dye, respectively.[3] Another common feature of the correlations is the sharp drop to unity at very short times (nanosecond range), which is due to photon antibunching.[5] The most pronounced difference between the two correlation functions is in the amplitude of an additional component decaying with a time constant of about 200 ns. The dependence of this am-

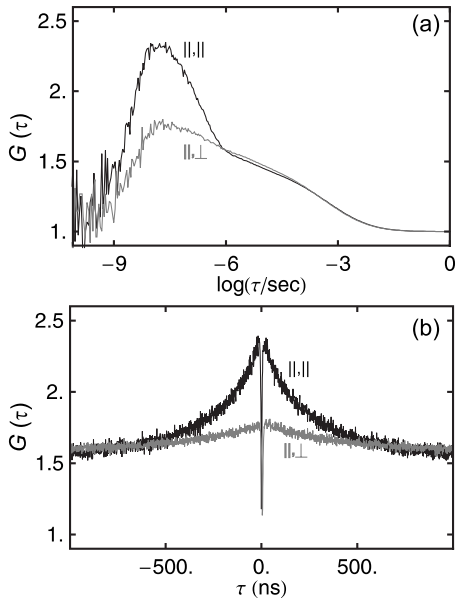

FIG. 3. FCS curves of 500 pM GroEL-bound rhodanese labeled with Alexa 488. The autocorrelation $G_{\parallel\parallel}(\tau)$ of the detected parallel polarized photons is shown in black, and the cross correlation $G_{\parallel\perp}(\tau)$ between parallel and perpendicularly polarized photons in gray. (a) Logarithmic plot, illustrating the large difference in amplitude from rotational dynamics, but coincidence of the correlations for $\tau > 1$ μs. (b) Linear plot for $\tau < 1$ μs.

plitude on the polarization components used for the correlation indicates that it is caused by diffusive rotational motion.[5] Whereas the rotational motion of the freely rotating dye would occur on a subnanosecond time scale, fluorescence anisotropy experiments indicate a substantial restriction of the rotational degree of freedom of the dye in the rhodanese-GroEL complex.[40] We thus observe the rotational diffusion of the entire rhodanese-GroEL complex. Remarkably, the relative amplitudes of the rotational components of $G_{\parallel\parallel}(\tau)$ and $G_{\parallel\perp}(\tau)$ are in good agreement with the values expected theoretically.[41]

Next, we demonstrate the ability of the HydraHarp 400 to obtain subpopulation-resolved correlation functions. In this experiment, we aimed to distinguish two polypeptides with different affinities for the molecular chaperone GroEL but present in the same solution. The sample contained 100 pM rhodanese labeled with Alexa 488, which forms a tight complex with unlabeled GroEL also present in the solution (see above), and 200 pM of polyproline-20 (Pro20),[42] a soluble peptide that does not interact with the chaperone. Pro20 was labeled with a dye pair (Alexa 488 as a donor and Alexa 594 as an acceptor) interacting via Förster resonance energy transfer (FRET),[42] resulting in a transfer efficiency of $E \approx 0.5$.[42] As a result, each time a Pro20 molecule diffuses through the confocal volume, a burst of photons is detected with about half of the photons emitted by the donor and half by the acceptor on average, whereas in the case of the chaperone-bound rhodanese, only donor photons are detected. Discriminating subpopulations with FRET is a common technique in single molecule spectroscopy,[43] which we combine here with FCS to obtain the different rotational behavior of chaperone-bound rhodanese and free Pro20.

For this purpose, we recorded parallel polarized donor photons with two detectors [for obtaining $G_{\parallel\parallel}(\tau)$]; on the

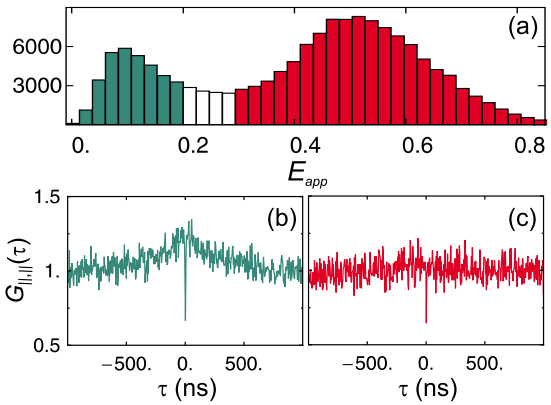

FIG. 4. (Color online) Subpopulation-resolved FCS of a mixture of 100 pM chaperone-bound rhodanese, labeled with Alexa 488, and 200 pM of Pro20, labeled with a FRET dye pair (donor, Alexa 488 and acceptor, Alexa 594). (a) Transfer efficiency histogram with two peaks corresponding to the two subpopulations. The ranges of E_{app} used for extracting the autocorrelation functions [(b) and (c)] of horizontally polarized donor emission $G_{\parallel\parallel}(\tau)$ are shaded correspondingly. (b) $G_{\parallel\parallel}(\tau)$ for the subpopulation of chaperone-bound rhodanese. (c) $G_{\parallel\parallel}(\tau)$ for the Pro20 subpopulation.

third and fourth detectors we measured the vertically polarized donor photons and the acceptor photons, respectively. From the recorded stream of photons, we identified photon bursts with more than fifty photons. In addition, the interphoton time during a burst had to be less than 100 μs. For each burst, we estimated the transfer efficiency by calculating $E_{app}=n_A/(n_D+n_A)$, where n_D and n_A are the total counts of donor photons and acceptor photons, respectively.[44] Two broad peaks are observable in a histogram of the values for E_{app} [Fig. 4(a)]: the one at low E_{app} corresponds to the donor-only labeled chaperone-bound rhodanese; the broad peak[45] centered at $E_{app} \approx 0.5$, corresponds to Pro20. Subpopulation-resolved autocorrelations $G_{\parallel\parallel}(\tau)$ were now obtained by correlating only those perpendicularly polarized donor photons of bursts with E_{app} values in the appropriate ranges [$E=0$ to $E=0.2$ for chaperone-bound rhodanese and $E=0.3$ to $E=0.8$ for the Pro20, see shaded bars in Fig. 4(a)]. The resulting autocorrelation functions are shown in Figs. 4(b) and 4(c). The subpopulation-specific correlation function for chaperone-bound rhodanese [Fig. 4(b)] is in agreement with the result shown in Fig. 3(b). Note that the decreased signal-to-noise ratio in Fig. 4(b) is due to the lower rhodanese concentration [100 pM instead of 500 pM in Fig. 3(b)] and to the conservative burst selection. Lower concentrations than in conventional FCS are necessary to ensure the proper discrimination of subpopulations. The autocorrelation of Pro20 [Fig. 4(c)] does not exhibit any rotational component on the nanosecond time scale because the peptide does not bind to the large chaperone and exhibits rotational components only in the picosecond to low nanosecond range.[42] The corresponding signal is therefore hidden in the photon antibunching component.

IV. CONCLUSION

Photon timing on independent channels has some striking advantages over the classical TAC based approach, especially in conjunction with time-tagged photon data collection. However, existing solutions are limited in terms of the number of independent input channels. Here, we have shown

a modular and scalable solution that overcomes several problems associated with a multichannel time-tagging TCSPC system. As opposed to the widely spread multiplexing TCSPC architectures, correlation artifacts because of dead times can be eliminated. In comparison to the most straightforward scaling by parallel operation of independent TCSPC units, we have eliminated the need for multiple synchronization channels, and furthermore we can obtain a single sorted data stream that enables efficient data analysis. Performance figures such as time resolution, linearity, dead time, and throughput were shown to be on the cutting edge of current state of the art.

In two illustrative applications, we showed that the simultaneous recording of photons on four channels with picosecond time resolution enables us to separate subpopulations using FRET and to obtain rapid dynamics on time scales shorter than the dead time of the detectors from subpopulation-specific correlation functions. With the possibility of correlating every possible combination of channels, dynamics on time scales ranging from picoseconds to seconds and above can be obtained from a single measurement. The use of the multichannel time-correlated photon counting system presented here greatly simplifies and extends the scope of single molecule measurements, which are of increasing importance, e.g., in the context of heterogeneous biological systems.[13,21,46–49]

ACKNOWLEDGMENTS

We thank Hagen Hofmann and Dominik Hänni for discussion and help with sample preparation. Initial instrument development was supported by IBB Berlin "Programm zur Förderung von Forschung, Innovation und Technologie," cofinanced by the EU fund for regional development (EFRE), contract number 10129879. Further work toward higher throughput is being supported by the BMBF Biophotoncis III program, Project Code 13N9271. D. N., F. H., and B. S. were supported by the Schweizerische Nationalfonds, the VolkswagenStiftung, and the Swiss National Center of Competence in Research for Structural Biology.

[1] J. R. Lakowicz, *Principles of Fluorescence Spectroscopy* (Springer, New York, 1999).
[2] J. Kalisz, Metrologia **41**, 17 (2004).
[3] R. Rigler and E. S. Elson, *Fluorescence Correlation Spectroscopy Theory and Applications* (Springer, Berlin, 2001).
[4] K. Schätzel, Inst. Phys. Conf. Ser. **77**, 175-184 (1985).
[5] M. Ehrenberg and R. Rigler, Chem. Phys. **4**, 390 (1974).
[6] P. Kask, P. Piksarv, and U. Mets, Eur. Biophys. J. **12**, 163 (1985).
[7] T. Basche, W. E. Moerner, M. Orrit, and H. Talon, Phys. Rev. Lett. **69**, 1516 (1992).
[8] P. Tinnefeld, K. D. Weston, T. Vosch, M. Cotlet, T. Weil, J. Hofkens, K. Mullen, F. C. De Schryver, and M. Sauer, J. Am. Chem. Soc. **124**, 14310 (2002).
[9] J. Sykora, K. Kaiser, I. Gregor, W. Bonigk, G. Schmalzing, and J. Enderlein, Anal. Chem. **79**, 4040 (2007).
[10] S. Fore, T. A. Laurence, C. W. Hollars, and T. Huser, IEEE J. Sel. Top. Quantum Electron. **13**, 996 (2007).
[11] P. Kask, P. Piksarv, U. Mets, M. Pooga, and E. Lippmaa, Eur. Biophys. J. **14**, 257 (1987).
[12] A. J. Berglund, A. C. Doherty, and H. Mabuchi, Phys. Rev. Lett. **89**, 068101 (2002).
[13] D. Nettels, I. V. Gopich, A. Hoffmann, and B. Schuler, Proc. Natl. Acad. Sci. U.S.A. **104**, 2655 (2007).
[14] C. Eggeling, J. R. Fries, L. Brand, R. Gunther, and C. A. M. Seidel, Proc. Natl. Acad. Sci. U.S.A. **95**, 1556 (1998).
[15] M. Wahl, R. Erdmann, K. Lauritsen, and H. J. Rahn, Proc. SPIE **3259**, 173 (1998).
[16] J. B. Edel and A. J. Demello, Appl. Phys. Lett. **90**, 053904 (2007).
[17] H. Z. Lin, S. R. Tabaei, D. Thomsson, O. Mirzov, P. O. Larsson, and I. G. Scheblykin, J. Am. Chem. Soc. **130**, 7042 (2008).
[18] C. Eggeling, S. Berger, L. Brand, J. R. Fries, J. Schaffer, A. Volkmer, and C. A. M. Seidel, J. Biotechnol. **86**, 163 (2001).
[19] H. P. Lu, *Methods in Molecular Biology* (Humana Press, Totowa, NJ, 2005), Vol. 305, p. 385.
[20] M. Wahl, I. Gregor, M. Patting, and J. Enderlein, Opt. Express **11**, 3583 (2003).
[21] D. Nettels and B. Schuler, IEEE J. Sel. Top. Quantum Electron. **13**, 990 (2007).
[22] D. C. Lamb, A. Schenk, C. Rocker, C. Scalfi-Happ, and G. U. Nienhaus, Biophys. J. **79**, 1129 (2000).
[23] M. Böhmer, M. Wahl, H. J. Rahn, R. Erdmann, and J. Enderlein, Chem. Phys. Lett. **353**, 439 (2002).
[24] F. Koberling, M. Wahl, M. Patting, H. J. Rahn, P. Kapusta, and R. Erdmann, Proc. SPIE **5143**, 181 (2003).
[25] U. Ortmann, T. Dertinger, M. Wahl, H. J. Rahn, M. Patting, and R. Erdmann, Proc. SPIE **5325**, 179 (2004).
[26] S. Felekyan, R. Kuhnemuth, V. Kudryavtsev, C. Sandhagen, W. Becker, and C. A. M. Seidel, Rev. Sci. Instrum. **76**, 083104 (2005).
[27] M. Wahl, H. J. Rahn, I. Gregor, R. Erdmann, and J. Enderlein, Rev. Sci. Instrum. **78**, 033106 (2007).
[28] M. Ghioni, A. Gulinatti, I. Rech, F. Zappa, and S. Cova, IEEE J. Sel. Top. Quantum Electron. **13**, 852 (2007).
[29] I. Rech, D. Resnati, S. Marangonia, M. Ghioni, and S. Cova, Proc. SPIE **6771**, 77113 (2007).
[30] I. Rech, S. Marangonia, D. Resnati, M. Ghioni, and S. Cova, J. Mod. Opt. **99999**(1), 1–8 (2008), http://www.informaworld.com/10.1080/09500340802318309. Accessed Dec. 18, 2008.
[31] D. J. S. Birch, D. McLoskey, A. Sanderson, K. Suhling, and A. S. Holmes, J. Fluoresc. **4**, 91 (1994).
[32] K. D. Weston, M. Dyck, P. Tinnefeld, C. Muller, D. P. Herten, and M. Sauer, Anal. Chem. **74**, 5342 (2002).
[33] D. P. Herten, A. Biebricher, M. Heilemann, T. Heinlein, C. Müller, P. Schlüter, P. Tinnefeld, K. D. Weston, M. Sauer, and J. Wolfrum, Recent Res. Dev. Appl. Phys. **7**, 345 (2004).
[34] H. Ta, A. Mogk, B. Bukau, and D.-P. Herten, 14th International Workshop on Single Molecule Spectroscopy and Ultrasensitive Analysis, Berlin, 2008 (unpublished).
[35] W. Becker, A. Bergmann, C. Biskup, L. Kelbauskas, T. Zimmer, N. Klöcker, and K. Benndorf, Proc. SPIE **4963**, 175 (2003).
[36] D. Knoll, K. E. Ehwald, B. Heinemann, A. Fox, K. Blum, H. Rucker, F. Furnhammer, B. Senapati, R. Barth, and U. Haak, Tech. Dig. - Int. Electron Devices Meet. **2002**, 783.
[37] F. Hillger, D. Hänni, D. Nettels, S. Geister, M. Grandin, M. Textor, and B. Schuler, Angew. Chem., Int. Ed. **47**, 6184 (2008).
[38] F. U. Hartl and M. Hayer-Hartl, Science **295**, 1852 (2002).
[39] R. H. Brown and R. Q. Twiss, Nature (London) **177**, 27 (1956).
[40] F. Hillger, D. Nettels, S. Dorsch, and B. Schuler, J. Fluoresc. **17**, 759 (2007).
[41] P. Kask, P. Piksarv, M. Pooga, U. Mets, and E. Lippmaa, Biophys. J. **55**, 213 (1989).
[42] B. Schuler, E. A. Lipman, P. J. Steinbach, M. Kumke, and W. A. Eaton, Proc. Natl. Acad. Sci. U.S.A. **102**, 2754 (2005).
[43] A. A. Deniz, T. A. Laurence, M. Dahan, D. S. Chemla, P. G. Schultz, and S. Weiss, Annu. Rev. Phys. Chem. **52**, 233 (2001).
[44] For getting more accurate estimates for the transfer efficiency, it would be necessary to correct for background photons, for different quantum yields of Alexa 488 and Alexa 594, and for the different detection efficiencies and crosstalk between the detection channels; B. Schuler, Methods Mol. Biol. **350**, 115 (2007) (for the mere discrimination between subpopulations, these corrections can be ignored).
[45] R. Best, K. Merchant, I. V. Gopich, B. Schuler, A. Bax, and W. A. Eaton, Proc. Natl. Acad. Sci. U.S.A. **104**, 18964 (2007).
[46] S. Weiss, Science **283**, 1676 (1999).
[47] G. Haran, J. Phys.: Condens. Matter **15**, R1291 (2003).
[48] X. Michalet, S. Weiss, and M. Jäger, Chem. Rev. (Washington, D.C.) **106**, 1785 (2006).
[49] B. Schuler and W. A. Eaton, Curr. Opin. Struct. Biol. **18**, 16 (2008).